



## ORIGINAL ARTICLE

# Visible light assisted photodegradation of 2,4-dinitrophenol using $\text{Ag}_2\text{CO}_3$ loaded phosphorus and sulphur co-doped graphitic carbon nitride nanosheets in simulated wastewater

Pankaj Raizada<sup>a,b,\*</sup>, Anita Sudhaik<sup>a</sup>, Pardeep Singh<sup>a,b</sup>, Pooja Shandilya<sup>a</sup>, Pankaj Thakur<sup>a,b</sup>, Hanbo Jung<sup>c</sup>

<sup>a</sup> School of Chemistry, Faculty of Basic Sciences, Shoolini University, Solan, HP, India

<sup>b</sup> Himalayan Centre for Excellence in Nanotechnology, Shoolini University. Solan, HP 173229, India

<sup>c</sup> Department of Materials Science & Engineering, Inha University, 100 Inha-ro, Namgu, Incheon 22212, Republic of Korea

Received 15 August 2018; accepted 3 October 2018

Available online 10 October 2018

## KEYWORDS

Co-doped graphitic carbon nitride;  
 $\text{Ag}_2\text{CO}_3$ ;  
Heterojunction formation;  
Enhanced photocatalysis;  
2,4-dinitrophenol degradation

**Abstract** Nowadays, hybrid photocatalysts are gaining importance due to their improved photocatalytic activity. In the present work,  $\text{Ag}_2\text{CO}_3$  was integrated phosphorous and sulphur co-doped g- $\text{C}_3\text{N}_4$  (PSGCN) photocatalyst ( $\text{Ag}_2\text{CO}_3$ /PSGCN) to minimize the recombination of photogenerated electron-hole pair. The co-doping resulted in band gap lowering in GCN leading to more visible light activity. Successful formation of well dispersed  $\text{Ag}_2\text{CO}_3$ /PSGCN suspension in water was established by zeta potential and Tyndall effect experiments. Phosphorous and sulphur co-doping in g- $\text{C}_3\text{N}_4$  resulted lowering of optical band gap that enhanced its photodegradation ability under visible light. The reduction in photogenerated electron-hole pair recombination was confirmed by photoluminescence and electrochemical impedance analysis. The photodegradation of 2, 4, dinitrophenol (DNP) followed pseudo first order kinetics and enhanced photocatalytic activity was due to semiconductor heterojunction for effective separation of electron-hole pair. Holes and hydroxyl radicals were two main oxidative species responsible for photodegradation of DNP into non-toxic products. COD, HPLC and LC-MS investigations were used to investigate the degradation fragment during DNP mineralization.  $\text{Ag}_2\text{CO}_3$ /PSGCN nanocomposite revealed high stability and recycle efficiency substantial for ten catalytic cycles.

© 2018 Production and hosting by Elsevier B.V. on behalf of King Saud University. This is an open access article under the CC BY-NC-ND license (<http://creativecommons.org/licenses/by-nc-nd/4.0/>).

\* Corresponding author at: School of Chemistry, Faculty of Basic Sciences, Shoolini University, Solan, HP, India.

E-mail address: [pankajchem1@gmail.com](mailto:pankajchem1@gmail.com) (P. Raizada).

Peer review under responsibility of King Saud University.



Production and hosting by Elsevier

## 1. Introduction

Semiconductor photocatalysis as a green technology has received a great attention for the elimination of organic pollutants under solar light irradiation (Bu et al., 2018; Shandilya et al., 2018a, 2018b, 2018c). The fabrication of photocatalysts with improved photocatalytic efficacy under visible-light irradiation has emerged as a promising and sustainable technology to tackle water pollution (Raizada et al., 2014a, 2014b; Shandilya et al., 2018a, 2018b, 2018c; Li et al., 2016). Many semiconductors such as TiO<sub>2</sub> and ZnO have been widely used as photocatalyst and exhibit substantial photocatalytic activity. However, wide band gap (~3.2 eV) and UV light activity (2–4% of the solar spectrum) restricts their practical application for solar (Zeng et al., 2015; Li et al., 2017). So, more efforts have been put toward the development of visible-light-responsive photocatalysts in order to utilize solar light in visible region (> 420 nm) that contains largest proportion of solar spectrum (approx. 45%) (Tian et al., 2017a, 2017b; Raizada et al., 2016). Therefore, fabrication of efficient photocatalyst that works well within visible region is a major thrust in field of environmental photocatalysis (Li et al., 2015a, 2015b, 2015c; Chen et al., 2017).

Very recently, graphitic carbon nitride (g-C<sub>3</sub>N<sub>4</sub>) as a stable allotrope of all carbon nitrides has emerged as a good photocatalyst under visible-light irradiation (Maeda et al., 2009; Zhu et al., 2014). The g-C<sub>3</sub>N<sub>4</sub> has high thermal stability, chemical inertness, appropriate band gap (band gap = 2.7 eV) and good catalytic activity (Mousavi et al., 2018; Sudhaik et al., 2018a, b). Despite of all these alluring properties, performance of g-C<sub>3</sub>N<sub>4</sub> materials is reduced by some drawbacks *i.e.* high recombination rate of photogenerated electron-hole pairs, low specific surface area and low visible light absorption (Sudhaik et al., 2018a,b). Recently, various strategies such as doping with non-metals and metals, coupling with graphene based materials and heterostructure formation with other semiconductors have been used to improve the photocatalytic activity of g-C<sub>3</sub>N<sub>4</sub> (Wu et al., 2018; Cao et al., 2017), etc.

Among all these approaches, doping is considered as one of the most efficient and appropriate method to enhance visible light activity and stability of g-C<sub>3</sub>N<sub>4</sub>. The doping with phosphorus results in more visible light absorption and improved photogenerated electron-hole separation. In-situ sulphur doping also enhances photocatalytic activity of g-C<sub>3</sub>N<sub>4</sub> via more absorption of visible light. Phosphorus doped g-C<sub>3</sub>N<sub>4</sub> was first prepared by Zhang et al. using dicyandiamide and [Bmim]PF<sub>6</sub> (ionic liquid) as starting material (Zhang et al., 2010). He et al. synthesized phosphorus doped g-C<sub>3</sub>N<sub>4</sub> using diammonium hydrogen phosphate as a precursor (Hu et al., 2014). Hong and coworkers fabricated mesoporous carbon nitride via in-situ sulphur doping using thiourea as starting material (Hong et al., 2012). sulphur-mediated method was used to encourage carbon nitride bulk condensation using amino group-free trithiocyanuric acid by Zhang and co-workers (Zhang et al., 2011).

As an another strategy, heterojunction formation with other semiconductors having appropriate redox potential of conduction and valence band also facilitates separation of photoinduced charge carriers in g-C<sub>3</sub>N<sub>4</sub> (Rosman et al., 2018; He et al., 2016). So far, many Ag based photocatalysts

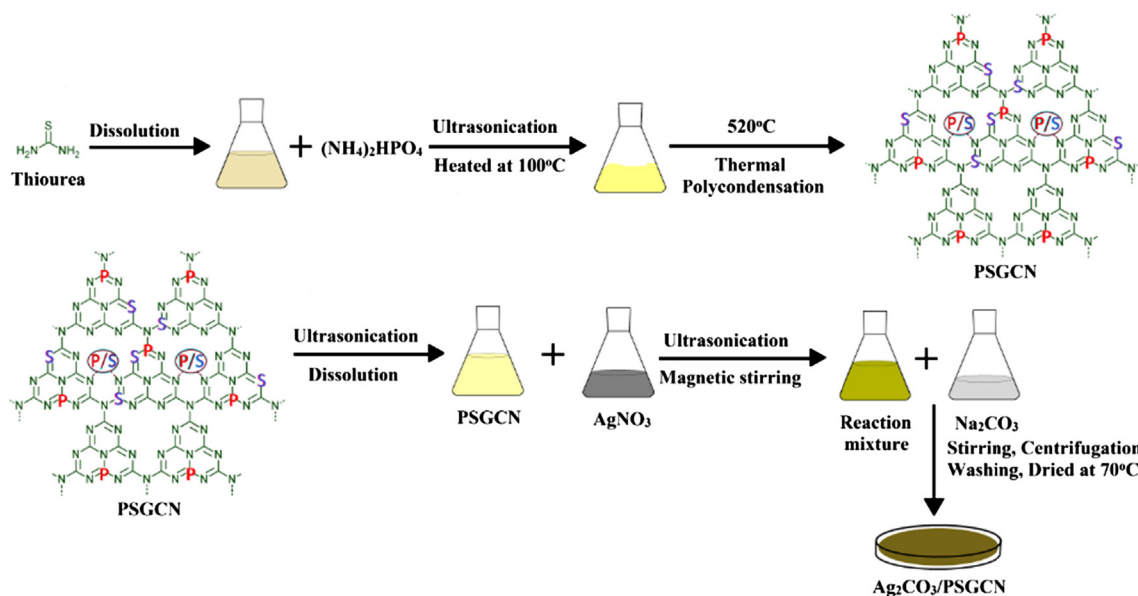
have been recognized as efficient photocatalysts under visible light for photocatalytic water purification such as Ag<sub>3</sub>PO<sub>4</sub> (Yi et al., 2010), Ag<sub>3</sub>VO<sub>4</sub> (Wang et al., 2014a, 2014b), AgX [X = Cl, Br and I] (Wang et al., 2011) and Ag<sub>2</sub>CO<sub>3</sub> (Xu et al., 2011; Yu et al., 2016). Ag<sub>2</sub>CO<sub>3</sub>, as a new visible light driven semiconducting material (band gap of 2.3 eV) is highly capable for degradation of organic pollutants under visible light (Dong et al., 2015). But unfortunately, aforementioned silver-based photocatalyst readily undergo photocorrosion during photocatalysis process, thus are photochemically unstable and deactivate during photocatalytic process (Li et al., 2015a, 2015b, 2015c). So, improvement in photocatalytic activity and stability of Ag<sub>2</sub>CO<sub>3</sub> is highly needed for efficient semiconductor photocatalytic systems. Dai et al. explored that use of silver nitrate as an electron acceptor reduced photocorrosion of Ag<sub>2</sub>CO<sub>3</sub> efficiently in the photocatalytic process (Dai et al., 2012). Graphene oxide-Ag<sub>2</sub>CO<sub>3</sub> composite was synthesized by Dong and his group with superior visible-light photocatalytic activity than bare Ag<sub>2</sub>CO<sub>3</sub> (Dong et al., 2014). Yu and his peer group synthesized Ag<sub>2</sub>O/Ag<sub>2</sub>CO<sub>3</sub> heterojunction with higher photocatalytic activity and stability than bare Ag<sub>2</sub>CO<sub>3</sub> (Yu et al., 2014). In this work, we have integrated phosphorus and sulphur co-doped g-C<sub>3</sub>N<sub>4</sub> with Ag<sub>2</sub>CO<sub>3</sub> via facile deposition-precipitation method to improve photocatalytic activity. The diammonium hydrogen phosphate was used as phosphorus source during PSGCN synthesis. 2, 4 nitrophenol (DNP) is considered as toxic and refractory pollutants. Moreover, it is partly biodegradable and cannot be removed by biological methods. In this work, DNP was chosen as target pollutant to evaluate photocatalytic activity of Ag<sub>2</sub>CO<sub>3</sub>/PSGCN nanocomposite. The efficient separation of photogenerated charge carriers in Ag<sub>2</sub>CO<sub>3</sub>/PSGCN nanocomposites accelerated photocatalytic reactions. The complete mineralization was attained under visible light and plausible mechanism for improved photocatalytic activity was put forward.

## 2. Experiment

### 2.1. Preparation of Ag<sub>2</sub>CO<sub>3</sub>/PSGCN photocatalyst

In this experiment, 3 g of thiourea was dissolved in 30 mL of deionised water and magnetically agitated for 30 min (Hong et al., 2012). To above solution, 0.06 g of (NH<sub>4</sub>)<sub>2</sub>HPO<sub>4</sub> was added and ultrasonicated for 15 min to form a homogeneous solution followed by heating for 25 min at 100 °C (Hu et al., 2014). After cooling, the product was crushed and annealed in closed crucible at 520 °C for 2 h (5 °C/min increment in temperature). The obtained yellow powder was labeled as phosphorus and sulphur co-doped graphitic carbon nitride (PSGCN) (Hu et al., 2015). In order to prepare SGCN, similar procedure was followed without the addition of (NH<sub>4</sub>)<sub>2</sub>HPO<sub>4</sub>. Phosphorus doped graphitic carbon nitride (PGCN) was fabricated by substituting thiourea with dicyandiamide. g-C<sub>3</sub>N<sub>4</sub> (GCN) was prepared using same procedure utilizing dicyandiamide as precursor in absence of (NH<sub>4</sub>)<sub>2</sub>HPO<sub>4</sub>.

Ag<sub>2</sub>CO<sub>3</sub>/PSGCN nanocomposite was synthesized via a simple chemical ion-exchange deposition method. Typically, 1 g of PSGCN was dissolved in 100 mL deionised water and ultrasonicated for 30 min. In another beaker AgNO<sub>3</sub> (0.015 g)



**Scheme 1** Preparation of  $\text{Ag}_2\text{CO}_3/\text{PSGCN}$  photocatalyst.

was dissolved in 20 mL deionized water and sonicated for 20 min (Scheme 1).  $\text{AgNO}_3$  solution was added dropwise to PSGCN solution to form homogeneous dispersion with continuous magnetic stirring to promote adsorption of  $\text{Ag}^+$  on PSGCN surface. Aqueous solution of  $\text{Na}_2\text{CO}_3$  (0.004 g in 20 mL) was slowly added to the above obtained solution. The reaction was sonicated for 45 min to obtain precipitates. The precipitates were separated and washed several times with deionized water and ethanol. Finally, precipitates were dried in hot air oven at  $70^\circ\text{C}$  and solid product was obtained. The attained solid product was grounded in pestle and mortar into fine powder form and labeled as  $\text{Ag}_2\text{CO}_3/\text{PSGCN}$  for further use.  $\text{Ag}_2\text{CO}_3$  was synthesized *via* same methodology without addition of PSGCN.

Nava Nano SEM-45 (USA) model system was employed to record scanning electron microscopy (SEM) images and model FP/5022-Tecna G2 20 S-TWIN (USA) operating at an accelerating voltage of 200 kV was used to attain transmission electron microscopy (TEM) images in vacuum conditions. Fourier-transform infrared (FTIR) analysis was executed on Perkin-Elmer Spectrometer (Spectrum RX-1) with KBr pellet. X-ray diffraction (XRD) analysis was performed using Panalytical's X'Pert Prodiffractometer with  $\text{CuK}\alpha$ -1 (45 kV/100 mA). Diffuse reflectance spectrometer (UV 3600, Shimadzu) was utilized to observe optical absorption spectra. The thickness and lateral size of  $\text{Ag}_2\text{CO}_3/\text{PSGCN}$  were evaluated by atomic force microscope (Dimensional Icon system, Bracer make). X-ray photoelectron spectroscopy (XPS) was performed on PHI Versa Probe II with AES using 24.63 W Al  $\text{K}\alpha$  radiations. Zeta potential was measured using Zetasizer Nano ZS90. The degradation fragments during mineralization process were recognized *via* high performance liquid chromatography analysis (Water HPLC, Austria) with Rheodyne manual injector kit and C18 column ( $5\ \mu\text{m}$ , 25 cm length and 7 mm diameter). 10% of methanol was taken as eluent during analysis. The LCMS spectra were obtained on JEOL GC/MATE II GC-MS with a high resolution data system.

## 2.2. Evaluation of photocatalytic activity of $\text{Ag}_2\text{CO}_3/\text{PSGCN}$

For the evaluation of photocatalytic activity of  $\text{Ag}_2\text{CO}_3/\text{PSGCN}$  nanocomposites, 2, 4 -dinitrophenol (DNP) was selected as a target pollutant. A slurry type photoreactor was used to examine DNP degradation under visible light (Pare et al., 2009, 2008). Prior to photocatalytic experiment, DNP solution containing catalyst was kept in dark for 20 min to attain adsorption and desorption equilibrium. The 35 W LED lamp was used as visible light source during photocatalytic reactions. During experiments, slurry composed of DNP and  $\text{Ag}_2\text{CO}_3/\text{PSGCN}$  photocatalyst suspension was continuously magnetic stirred under visible light irradiation exposure. 2 mL of aliquot was withdrawn, centrifuged and analyzed spectrophotometrically at 280 nm to check the degradation of DNP. The closed reflux method was used for the determination of chemical oxygen demand (APHA, 1985). The dissolved carbon dioxide was examined by titrating sample with NaOH using phenolphthalein as indicator. The removal efficiency was calculated using Eq. (1):

$$\% \text{ removal efficiency} = \frac{C_0 - C_t}{C_0} \quad (1)$$

where,  $C_0$  is the initial concentration of sample/COD and  $C_t$  is instant concentration of sample/COD in reaction solution.

## 3. Results and discussion

### 3.1. Characterization of $\text{Ag}_2\text{CO}_3/\text{PSGCN}$ photocatalyst

#### 3.1.1. FESEM and TEM analysis

FESEM and TEM analysis of GCN, PGCN, SGCN, PSGCN and  $\text{Ag}_2\text{CO}_3/\text{PSGCN}$  are depicted in Figs. 1 and 2. Fig. 1a revealed porous nature of graphitic carbon nitride highly suited for adsorption of organic/inorganic molecules. FESEM

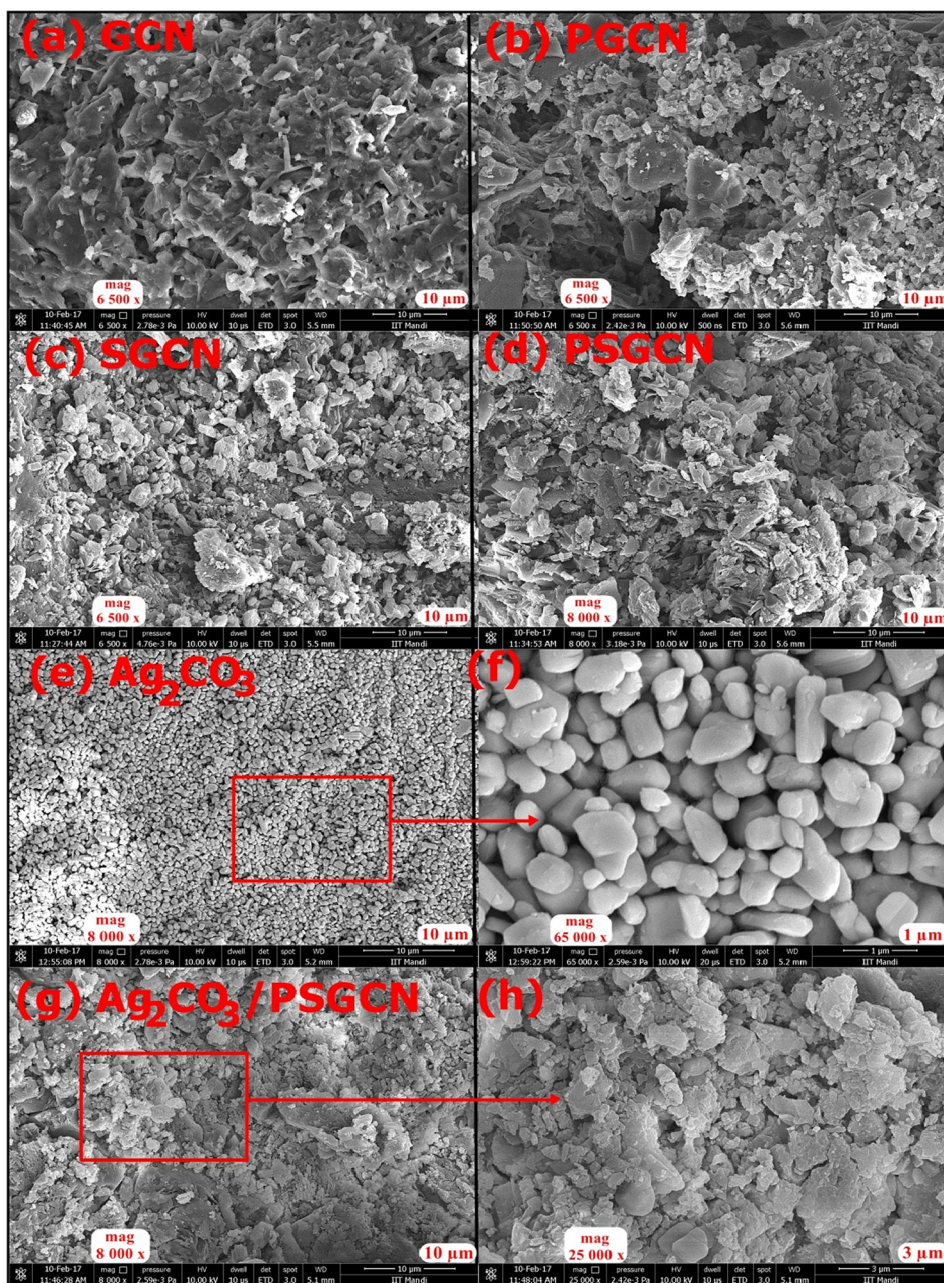


**Fig. 1** (a–h). SEM image of (a) GCN, (b) PGCN, (c) SGCN, (d) PSGCN, (e)  $\text{Ag}_2\text{CO}_3$ , (f) Magnified view of selected area of (e), (g)  $\text{Ag}_2\text{CO}_3/\text{PSGCN}$  and (h) magnified view of selected area of (h).

images of GCN showed irregular and lamellar structure with possibility to favor stacking of  $\text{Ag}_2\text{CO}_3$  its surface. The layered structure diminished due to presence of phosphorous and sulphur in GCN indicating that doping had reduced crystal growth of GCN as shown in Fig. 1b–d (Wang et al., 2014a, 2014b). FESEM image of  $\text{Ag}_2\text{CO}_3$  revealed different shaped agglomerated nanoparticles Fig. 1e–f. The distribution and stacking of  $\text{Ag}_2\text{CO}_3$  onto PSGCN surface was clearly seen. Fig. 2a–d shows TEM images of GCN, PSGCN,  $\text{Ag}_2\text{CO}_3$  and  $\text{Ag}_2\text{CO}_3/\text{PSGCN}$ . Fig. 2a and b revealed that GCN had thin sheet like structure and composed of nanostructure with straticulate and plicate shapes. Fig. 2c and d showed distribution of  $\text{Ag}_2\text{CO}_3$  nanoparticles onto  $\text{Ag}_2\text{CO}_3/\text{PSGCN}$ .  $\text{Ag}_2\text{CO}_3$

were successfully dispersed over phosphorous sulphur doped GCN sheet surface.

### 3.1.2. XRD and FTIR analysis of $\text{Ag}_2\text{CO}_3/\text{PSGCN}$

Fig. 3 displayed X-ray diffraction (XRD) patterns of GCN, PGCN, SGCN, PSGCN,  $\text{Ag}_2\text{CO}_3$  and  $\text{Ag}_2\text{CO}_3/\text{PSGCN}$  samples. The XRD pattern of GCN revealed two peaks at approximately  $13.1^\circ$  and  $27.4^\circ$  (Jiang et al., 2017a, 2017b; Malik et al., 2017). The small reflection peak was related to in-plane structural packing motif of tri-s-triazine units (1 0 0) and the dominant peak was connected to the interlayer stacking reflection of the aromatic segments (0 0 2) planes of the tetragonal phase of GCN (JCPDS 87-1526) (Malik et al., 2018, Ren et al., 2015).

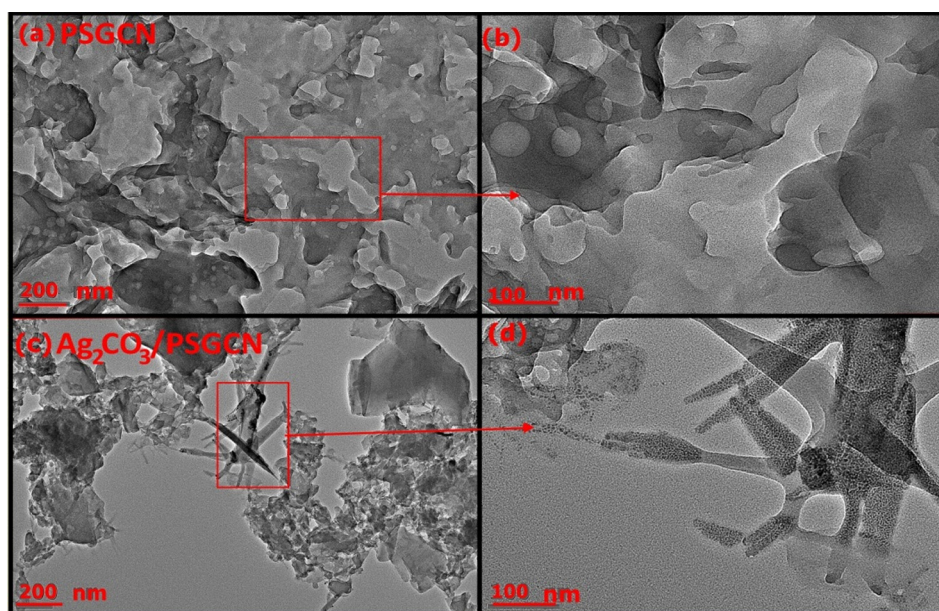


**Fig. 2** (a) TEM images of PSGCN, (b) enlarged view of selected area of figure (a), (c) TEM image of Ag<sub>2</sub>CO<sub>3</sub>/PSGCN and (d) enlarged view of selected area of figure (c).

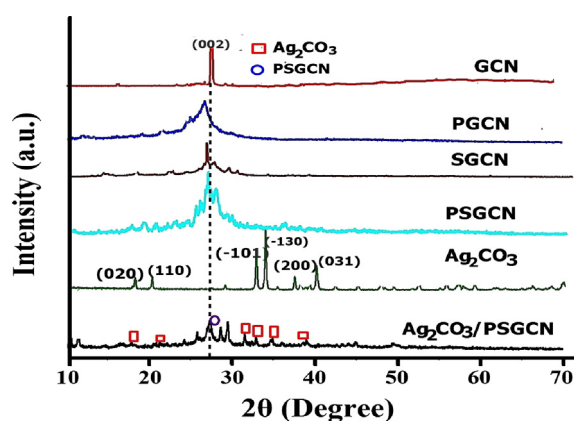


**Fig. 3** XRD analysis of Ag<sub>2</sub>CO<sub>3</sub>/PSGCN, Ag<sub>2</sub>CO<sub>3</sub>, PSGCN, PGCN, SGCN and GCN.

In PSGCN, peak at 27.4° was shifted to 27.7° due to increase in inter-planar stacking distance (Sun et al., 2018). The pure Ag<sub>2</sub>CO<sub>3</sub> displayed sharp diffraction peaks at 2θ = 18.56, 20.54°, 32.61°, 33.67°, 37.08°, 39.59° and 51.38° which ascribed to (0 2 0), (1 1 0), (1 0 1), (1 3 0), (2 0 0), (0 3 1) and (1 5 0) planes, respectively (JCPDS 26-0339) (Li et al., 2015a, 2015b, 2015c). The XRD pattern of Ag<sub>2</sub>CO<sub>3</sub>/PSGCN nanocomposite displayed characteristic peaks of both Ag<sub>2</sub>CO<sub>3</sub> and PSGCN which confirmed the successful formation of Ag<sub>2</sub>CO<sub>3</sub>/PSGCN. Additionally, FTIR analysis was used to find major functional groups in Ag<sub>2</sub>CO<sub>3</sub>/PSGCN and results are presented in Fig. 4. The FTIR spectra of GCN depicts stretching of typical aromatic C-N heterocycles in the region of 1200–1650 cm<sup>-1</sup> and the breathing mode of tri-s-triazine units (heptazine rings) at 808–810 cm<sup>-1</sup> (Lakhi et al., 2017). The peak around 2200 cm<sup>-1</sup> confirmed presence of cyano terminal groups (CN) in GCN. In case of PGCN, SGCN and PSGCN, charac-

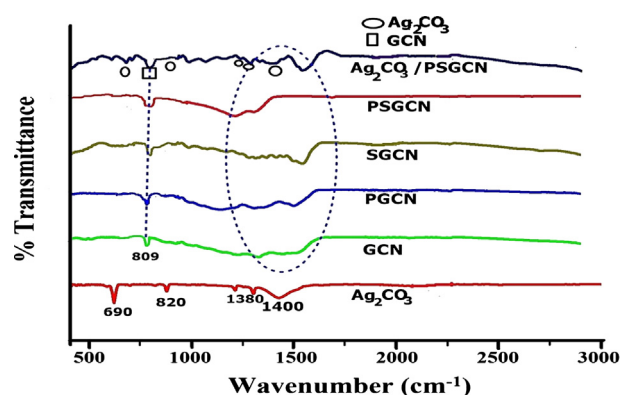


**Fig. 4** FTIR analysis of Ag<sub>2</sub>CO<sub>3</sub>/PSGCN, PSGCN, SGCN, PGCN, GCN and Ag<sub>2</sub>CO<sub>3</sub>.

teristic peaks of GCN were observed. However, no P-N and S-N peaks were observed and these findings are consistent with work by Wang and his research group (Tian et al., 2018; Jiang et al., 2017a, 2017b). In FTIR spectra of pure Ag<sub>2</sub>CO<sub>3</sub>, absorption peaks of CO<sub>3</sub><sup>2-</sup> were observed at 690, 820, 1380 and 1400 cm<sup>-1</sup> (Song et al., 2014). The sharp peak at 1380 cm<sup>-1</sup> was due to existence of nitrate impurities as AgNO<sub>3</sub> precursor used for Ag<sub>2</sub>CO<sub>3</sub> synthesis. The FTIR spectrum of Ag<sub>2</sub>CO<sub>3</sub>/PSGCN displayed characteristic peaks of both Ag<sub>2</sub>CO<sub>3</sub> and PSGCN. FTIR analysis indicated formation of Ag<sub>2</sub>CO<sub>3</sub>/PSGCN nanocomposites.

### 3.1.3. XPS analysis.

XPS analysis was employed to determine oxidation state and surface chemical composition of elements present in Ag<sub>2</sub>CO<sub>3</sub>/PSGCN (Fig. 5a–g). The atomic percentage of 46.1%, 33.7%, 10.2%, 4.8%, 3.7% and 1.5% were found for nitrogen, carbon, oxygen, sulphur, phosphorus and silver in Ag<sub>2</sub>CO<sub>3</sub>/

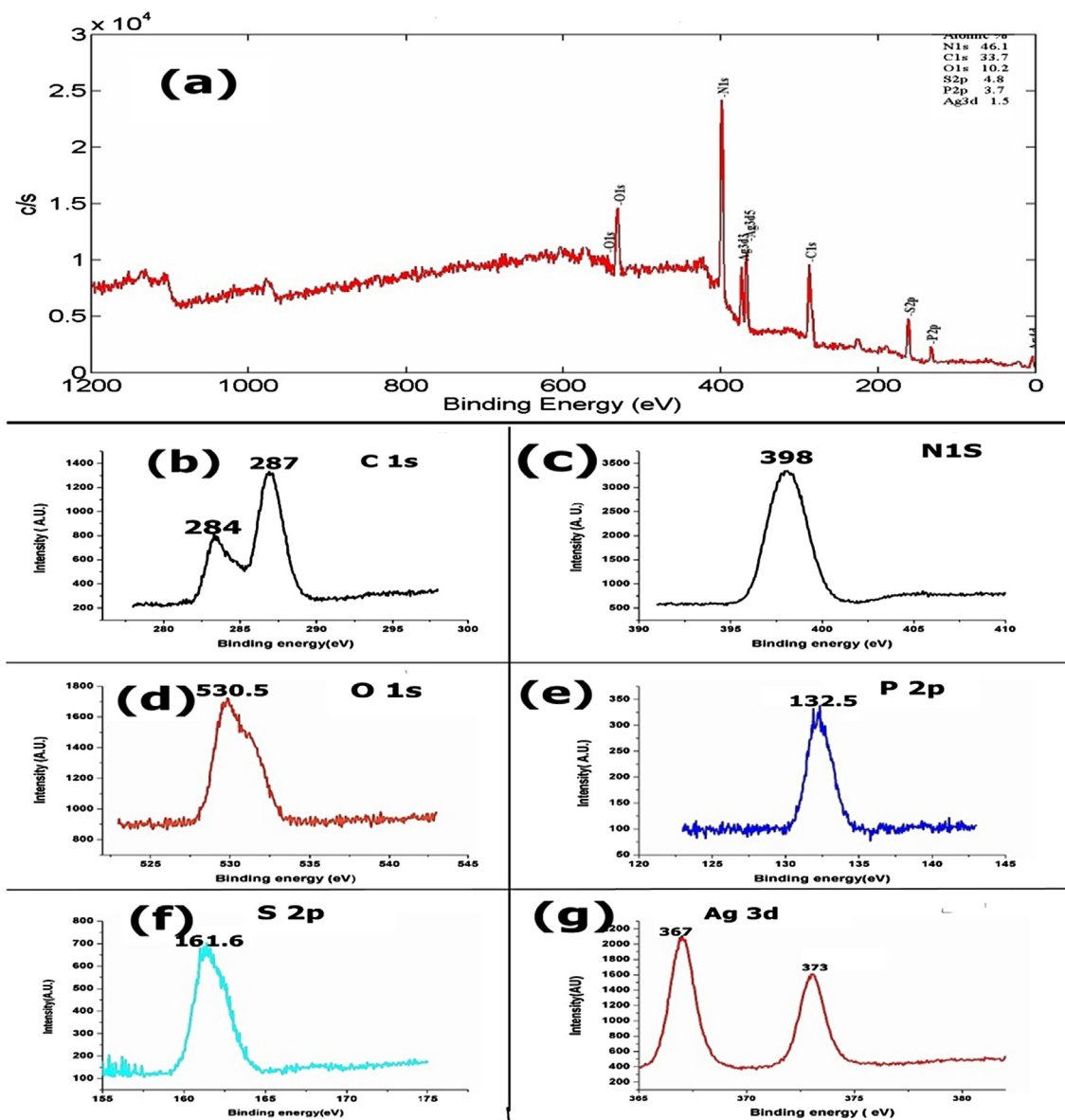


Fig. 5 XPS (a) whole spectrum of Ag<sub>2</sub>CO<sub>3</sub>/PSGCN, (b) C1s, (c) N 1s, (d) O1s, (e) P 2p, (f) S2p and (g) Ag 3d spectra.

PSGCN nanocomposite (Fig. 5a). For C1s, peaks located at 284 and 287 eV were attributed to sp<sup>2</sup> hybridized carbon atom bonded to nitrogen [C (C-(N)<sub>3</sub>)] in GCN (Fig. 5b) (Yang et al., 2014; Ge and Han, 2012). In Fig. 5c, main peak of N 1s at 398 eV assigned to sp<sup>2</sup>-hybridized aromatic nitrogen atom bonded to two carbon atoms in triazine rings (C = N-C) and confirmed the presence of sp<sup>2</sup>-bonded GCN (Malik et al., 2018). In O1s spectra (Fig. 5d), the binding energy at 530.5 eV corresponded to O-H and ascribed to O in Ag<sub>2</sub>CO<sub>3</sub> (Bigelow, 1988). In Fig. 5e, the peak at 132.5 eV was allocated to P-N bonds formed due to replacement of carbon in GCN lattice. For S 2p, the peak at 141.6 eV was detected due to formation of C-S bond in PSGCN (Fig. 5f). Chen et al. also fabricated S doped GCN and suggested that the binding energy at 161.6 eV was due to replacement of nitrogen by sulphur (Liu et al., 2010). The Ag 3d<sub>5/2</sub> and Ag 3d<sub>3/2</sub> peaks were present at 367 eV and 373 eV, respectively (Fig. 5g). These peaks were due to presence of Ag<sup>+</sup> ion in Ag<sub>2</sub>CO<sub>3</sub>.

### 3.1.4. Band gap, photoluminescence, BET and pH<sub>pzc</sub> analysis.

UV-visible diffuse reflectance spectroscopy was used to analyze optical properties of GCN, Ag<sub>2</sub>CO<sub>3</sub>, PSGCN and Ag<sub>2</sub>CO<sub>3</sub>/PSGCN (Fig. 6a). GCN, Ag<sub>2</sub>CO<sub>3</sub>, PSGCN and Ag<sub>2</sub>CO<sub>3</sub>/PSGCN had maximal absorption at 460, 560, 475 and 590 nm, respectively. In PSGCN, absorption edge was red shifted from 460 nm to 475 nm. The shift indicated the integration of P and S atoms into GCN lattice which resulted in more absorption of visible light to produce more photogenerated electron-hole pairs (Jiang et al., 2017a, 2017b; Guo et al., 2016). In case of Ag<sub>2</sub>CO<sub>3</sub>/PSGCN nanocomposites, heterostructure formation resulted in trapping of more UV and visible light with absorption peak at 590 nm. The apparent red shift was observed in absorption maximum of Ag<sub>2</sub>CO<sub>3</sub>/PSGCN nanocomposite as compared to GCN and PSGCN (Dai et al., 2012). The red shift confirmed successful formation of Ag<sub>2</sub>CO<sub>3</sub>/PSGCN nanocomposite. The optical band gap of

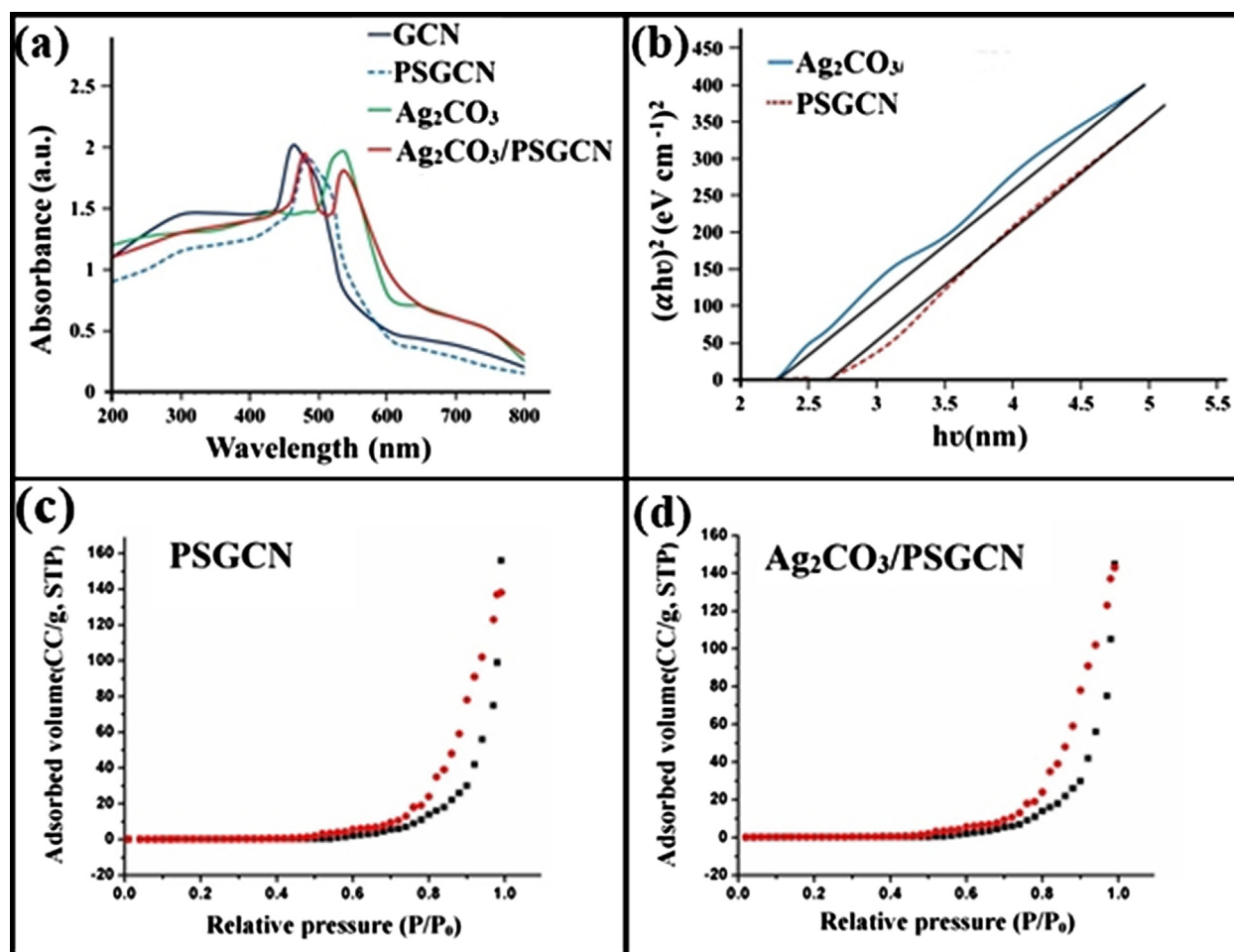


Fig. 6 (a–d): (a) UV–visible spectrum, (b) Tauc plot of GCN, PSGCN, Ag<sub>2</sub>CO<sub>3</sub> and Ag<sub>2</sub>CO<sub>3</sub>/PSGCN, (c and d) BET isotherm of PSGCN and Ag<sub>2</sub>CO<sub>3</sub>/PSGCN.

as prepared photocatalysts was calculated using following equation (Jing et al., 2017):

$$E_g = 1240/\lambda \quad (2)$$

where  $\lambda$  is absorption maximum of prepared photocatalysts. So, the respective band gaps of GCN, PSGCN and Ag<sub>2</sub>CO<sub>3</sub> were found to be 2.70, 2.6 and 2.3 eV, which were consistent with previous literature (Fig. 7b) (Dai et al., 2012). The P and S co-doping reduces band gap of GCN, implying the incorporation of P and S in GCN lattice. Decrease in band gap was in accordance with previous reports and responsible for increased visible light absorption.

The specific surface area of photocatalyst plays an important role in adsorption assisted photocatalytic activity. Fig. 6c and d demonstrated nitrogen adsorption-desorption isotherms of PSGCN and Ag<sub>2</sub>CO<sub>3</sub>/PSGCN nanoparticles. The acquired isotherms possessed type III classification that verified unrestricted multilayer formation process and these lateral interactions among adsorbed molecules are strong as comparison to interaction between the adsorbent surface and adsorbate in photocatalyst. PSGCN and Ag<sub>2</sub>CO<sub>3</sub>/PSGCN nanoparticles had specific area of 81.0 m<sup>2</sup>/g and 70.0 m<sup>2</sup>/g, respectively. The loading of Ag<sub>2</sub>CO<sub>3</sub> nanoparticles on PSGCN reduced specific area due to presence of Ag<sub>2</sub>CO<sub>3</sub> in inner layers

or pores of PSGCN that instigated lesser agglomeration of Ag<sub>2</sub>CO<sub>3</sub> (Xu et al., 2014). The pH of zero point charge (pH<sub>pzc</sub>) as an important parameter as well as a function of pH was used for the determination of photocatalyst surface charge. In the present work, pH<sub>pzc</sub> of Ag<sub>2</sub>CO<sub>3</sub>/PSGCN nanocomposite was found to be 7.1 (Fig. S1).

### 3.1.5. AFM and dispersion experiment

Atomic force microscopy was used to investigate thickness of Ag<sub>2</sub>CO<sub>3</sub>/PSGCN nanocomposite. The AFM images and corresponding height profiles are displayed in Fig. 7a and b. PSGCN nanocomposite exhibited 3–4 layered sheet like arrangement with thickness < 3.0 nm (Adams and Blaedel, 1959). AFM results were also supported by SEM and TEM analysis in present work. The zeta potential of Ag<sub>2</sub>CO<sub>3</sub>/PSGCN nanocomposite was below -27 mV at pH 12 which confirmed the formation of stable colloidal suspension. Ag<sub>2</sub>CO<sub>3</sub>/PSGCN could remain dispersed in water for 6 h (Fig. 7d). Tyndall effect was also observed for colloidal nature of Ag<sub>2</sub>CO<sub>3</sub>/PSGCN nanocomposite by dispersing Ag<sub>2</sub>CO<sub>3</sub>/PSGCN nanocomposite in water with red beam of laser point (Fig. 7e and f). Although in case of water, no Tyndall effect was observed. The higher dispersibility of Ag<sub>2</sub>CO<sub>3</sub>/PSGCN

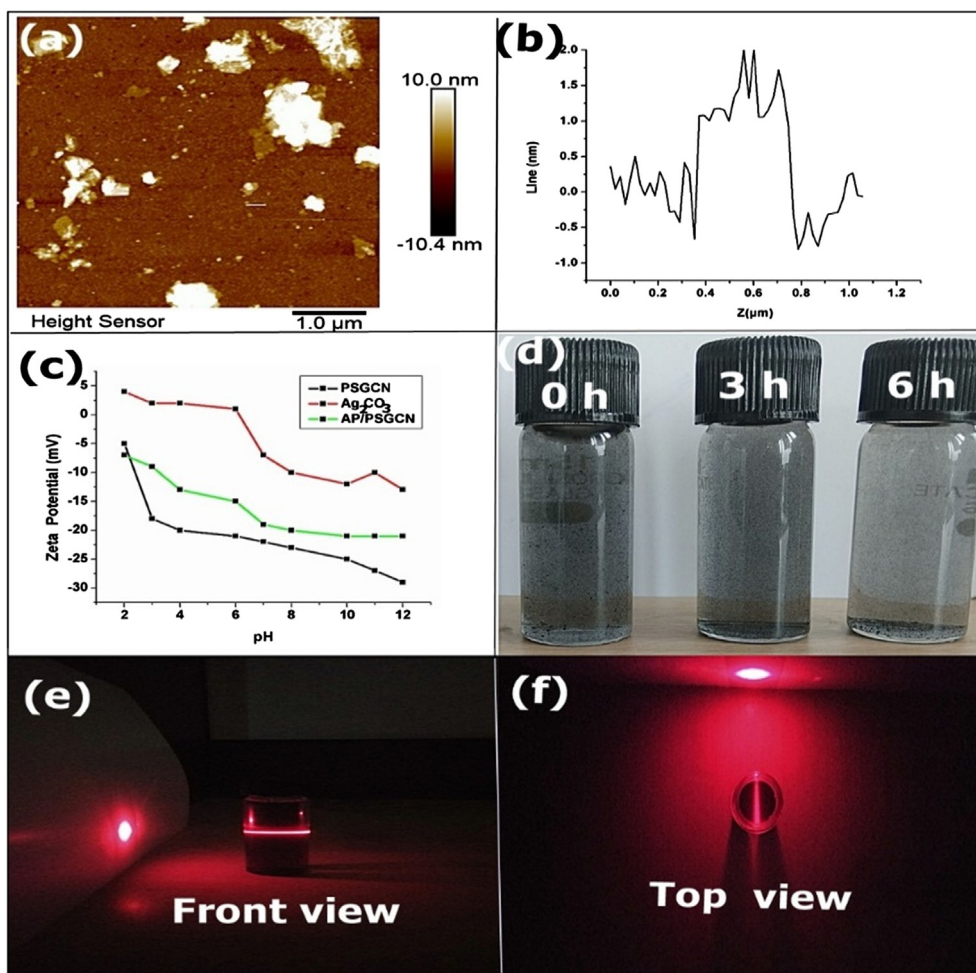


**Fig. 7** (a) AFM analysis Ag<sub>2</sub>CO<sub>3</sub>/PSGCN (b) Z line profile for Ag<sub>2</sub>CO<sub>3</sub>/PSGCN, (c) zeta potential of PSGCN, Ag<sub>2</sub>CO<sub>3</sub> and Ag<sub>2</sub>CO<sub>3</sub>/PSGCN and (d) dispersion effect and (e and f) Tyndall effect in Ag<sub>2</sub>CO<sub>3</sub>/PSGCN.

nanocomposite was beneficial for effective slurry type photoreactor.

### 3.2. Photocatalytic degradation of DNP using Ag<sub>2</sub>CO<sub>3</sub>/PSGCN nanocomposite

#### 3.2.1. Screening experiment and kinetics of DNP degradation

The photocatalytic activity of as-prepared Ag<sub>2</sub>CO<sub>3</sub>, GCN, PGCN, SGCN, PSGCN and Ag<sub>2</sub>CO<sub>3</sub>/PSGCN photocatalysts was calculated by screening experiments. Time profile for DNP degradation at concentration of  $1 \times 10^{-4}$  mol dm<sup>-3</sup> and 50 mg/100 mL of catalyst loading was shown in Fig. 8a. The decreasing order of DNP removal efficiency was as follows: Ag<sub>2</sub>CO<sub>3</sub>/PSGCN (98%) > PSGCN (71%) > Ag<sub>2</sub>CO<sub>3</sub> (66%) > PGCN (62%) = SGCN (62%) > GCN (58%) while in the absence of any photocatalyst, plain photolysis showed negligible effect on DNP removal. Langmuir Hinshelwood model was used to investigate kinetics of photodegradation process and following equation was applied to explore photocatalytic degradation of DNP (Priya et al., 2016; Singh et al., 2014).

$$-\frac{dC}{dt} = kt \quad (3)$$

where C signified DNP concentration at time t and k connoted rate constant. On integration above by limits (0, C<sub>0</sub>) and (t, C), we get Eqs. (4) and (5).

$$-\ln\left(\frac{C_t}{C_0}\right) = kt \quad (4)$$

$$\ln\left(\frac{C_0}{C_t}\right) = kt \quad (5)$$

$\ln(C_0/C_t)$  versus time (t) graph was plotted for DNP degradation and overall photodegradation process followed pseudo first order kinetics. Ag<sub>2</sub>CO<sub>3</sub>/PSGCN, PSGCN, Ag<sub>2</sub>CO<sub>3</sub>, PGCN, SGCN and GCN had rate constants *i.e.* 0.087, 0.047, 0.045, 0.30 and 0.29 min<sup>-1</sup>, respectively (Table 1). Ag<sub>2</sub>CO<sub>3</sub>/PSGCN had approximately two fold higher catalytic activity than other used photocatalysts. P and S co-doping enhanced photodegradation efficacy of GCN, PGCN and SGCN due to enhanced solar light adsorption and reduced photogenerated electron-hole pair recombination. Ag<sub>2</sub>CO<sub>3</sub>/PSGCN nanocomposite was most effective photocatalyst for DNP degradation due high separation of photogenerated carriers. The photoluminescence analysis was used to explore charge separation efficiency. PL emission peak of Ag<sub>2</sub>CO<sub>3</sub> was recorded at 560 nm (Fig. 8b). The higher peak intensity

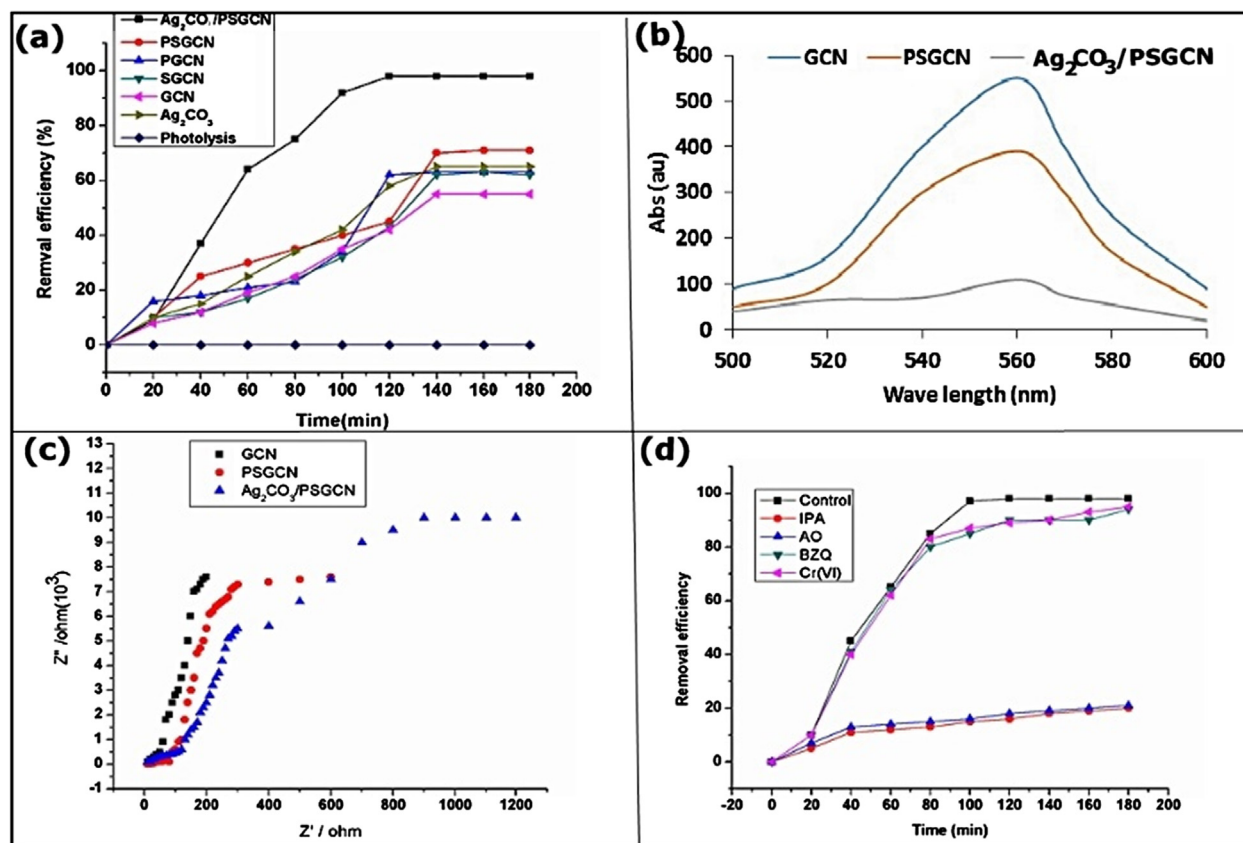


**Fig. 8** (a–d): (a) Photo removal of DNP under various reaction conditions, (b) PL spectra of photocatalyst (c) Reaction parameter: [DNP] =  $1.0 \times 10^{-3}$  mol dm<sup>-3</sup>; [photocatalyst] = 50 mg/100 mL; initial reaction pH = 4.0 and Light intensity = 750 lx. (d) Effect of scavengers on photodegradation of DNP photocurrent response of photocatalyst.

**Table 1** Rate constant the photodegradation of phenol. Reaction conditions: [DNP] =  $1 \times 10^{-3}$  mol dm<sup>-3</sup>; [catalyst] = 50 mg/100 mL; initial reaction pH = 4.0; Time = 120 min and Solar light intensity = 750 lx.

Photocatalyst	Rate constant ( $k_1$ ) min <sup>-1</sup>	R <sup>2</sup>	% efficiency
Ag <sub>2</sub> CO <sub>3</sub> /PSGCN	0.087	0.97	98
PSGCN	0.047	0.98	71
PGCN	0.036	0.96	62
SGCN	0.030	0.97	62
GCN	0.029	0.98	58
Ag <sub>2</sub> CO <sub>3</sub>	0.045	0.97	66

was related to more recombination rate of photogenerated electrons-hole pair (Jiang et al., 2017a, 2017b). The PL emission peak of Ag<sub>2</sub>CO<sub>3</sub>/PSGCN had lower intensity than Ag<sub>2</sub>CO<sub>3</sub>. It confirmed separation of photogenerated electron-hole pairs by reducing recombination of photogenerated electron and hole pair. Fig. 8c illustrates EIS spectra of GCN, PSGCN and Ag<sub>2</sub>CO<sub>3</sub>/PSGCN. The trend of relative arc size for three electrodes was: Ag<sub>2</sub>CO<sub>3</sub>/PSGCN > PSGCN > GCN. The highest arc size in Ag<sub>2</sub>CO<sub>3</sub>/PSGCN indicated lower rate of recombination of photogenerated electron hole pairs. The P and S co-doping of GCN followed by heterostructure formation with silver carbonate had resulted improved photogenerated charge carriers separation (Hu et al., 2018).

### 3.2.2. Reactive species generation and proposed mechanism for DNP degradation

The hydroxyl radicals (OH<sup>•</sup>), superoxide radicals (O<sub>2</sub><sup>•-</sup>), holes (h<sub>VB</sub><sup>+</sup>) and electrons (e<sub>CB</sub><sup>-</sup>) are main reactive species generated during photocatalytic degradation of aqueous phase pollutants. In present work, scavenging experiments were accomplished using isopropyl alcohol (IPA), benzoquinone (BZQ), ammonium oxalate(AO) and Cr(VI) ions as OH<sup>•</sup>, O<sub>2</sub><sup>•-</sup>, h<sub>VB</sub><sup>+</sup> and e<sub>CB</sub><sup>-</sup> scavengers, respectively (Zhang et al., 2015; Raizada et al., 2017a, 2017b). In Fig. 8d, it was observed that addition of AO reduced removal efficiency from 98% to 20%. The reduction in removal efficiency clearly ascertained photogenerated holes (h<sup>+</sup>) as main reactive species during photocatalytic degradation process. For Ag<sub>2</sub>CO<sub>3</sub>/PSGCN, removal efficacy was reduced to 21% from 98% on addition of IPA to reaction mixture. Though, in case of benzoquinone (BZQ) and Cr(VI), negligible decrease in removal efficiency was obtained thus established ignorable role of O<sub>2</sub><sup>•-</sup> radicals and e<sub>CB</sub><sup>-</sup> (Fig. 8d). There was a sharp decrease in removal efficiency on addition of IPA and AO. While in case of BZQ and Cr(VI), no significant decrease in removal efficiency was noticed. The obtained trend clearly inferred that OH<sup>•</sup> and holes were two main reactive species in Ag<sub>2</sub>CO<sub>3</sub>/PSGCN assisted photodegradation of DNP.

In present study, valence band (VB) and conduction band potential (CB) were calculated according to following equations (Wang et al., 2009; Kim et al., 2010):

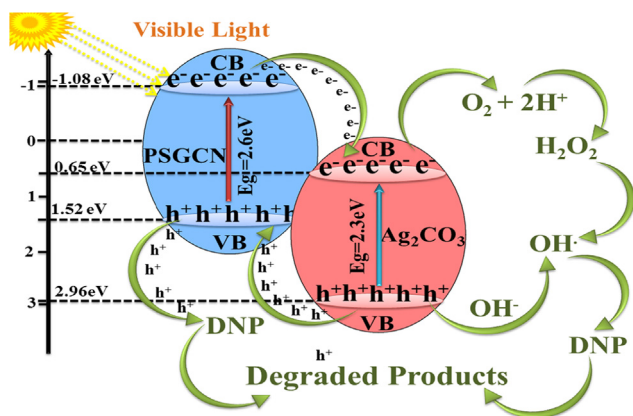


**Fig. 9** Mechanism for enhanced photocatalytic activity of Ag<sub>2</sub>CO<sub>3</sub>/PSGCN.

$$E_{VB} = \chi - E^e + 0.5E_g \quad (6)$$

$$E_{CB} = E_{VB} - E_g \quad (7)$$

where  $\chi$  is electronegativity of photocatalyst,  $E^e$  denoted energy of free electron at hydrogen scale (4.5 eV) and  $E_g$  designated for band gap of photocatalyst. The respective values of  $E_g$  and  $\chi$  for Ag<sub>2</sub>CO<sub>3</sub> are 2.3 and 6.13 eV. In PSGCN,  $E_g$  and  $\chi$  were 2.6 and 4.73 eV, respectively. The CB and VB positions of Ag<sub>2</sub>CO<sub>3</sub> were obtained as 0.65 and 2.96 eV, respectively. While CB and VB positions of PSGCN were found to be -1.08 and 1.52 eV (Zhang et al., 2013). The photogenerated electron from CB of PSGCN were transferred to CB of Ag<sub>2</sub>CO<sub>3</sub>. This was due to more negative potential of CB of PSGCN than that of O<sub>2</sub>/O<sub>2</sub><sup>-</sup> ( $E_0$  (O<sub>2</sub>/O<sub>2</sub><sup>-</sup>) = -0.33 eV/NHE). Similarly, holes (h<sup>+</sup>) in VB of Ag<sub>2</sub>CO<sub>3</sub> were shifted to that of PSGCN due to strong interfacial contact and more positive VB level of Ag<sub>2</sub>CO<sub>3</sub> than PSGCN (Jiang et al., 2012; Tian et al., 2015). The photoexcited electrons in CB of Ag<sub>2</sub>CO<sub>3</sub> could not react with O<sub>2</sub> to produce O<sub>2</sub><sup>-</sup> due to positive potential of CB of Ag<sub>2</sub>CO<sub>3</sub> (0.67 eV). However, These just combined with O<sub>2</sub> and H<sup>+</sup> ions in water to form H<sub>2</sub>O<sub>2</sub> and ultimately producing hydroxyl radicals (Eqs. (8) and (9))



So, photogenerated electron-hole pair recombination was diminished and improvement in photocatalytic activity of Ag<sub>2</sub>CO<sub>3</sub>/PSGCN nanocomposite was observed. The holes h<sup>+</sup> and ·OH radicals were the two main reactive species that play essential roles for DNP photodegradation. On the basis of above results, a possible mechanism for photodegradation of DNP by Ag<sub>2</sub>CO<sub>3</sub>/PSGCN photocatalyst was proposed in Fig. 9.

### 3.2.3. Effect of photocatalyst dose, initial DNP concentration and initial pH of reaction solution

In present work, photocatalyst dose was varied from 10 mg/50 mL to 70 mg/50 mL. The rate constant increased from 0.027 to 0.087 min<sup>-1</sup> with increase in catalyst loading from 10 mg/50 mL to 40 mg/50 mL (Fig. S2a and Table S1). The number of active sites for photodegradation process also increased with increase in catalyst dose (Raizada et al.,

2014a, 2014b). Though, above optimal loading, light scattering, turbidity and agglomeration subdued photoactive volume and diminished removal efficiency. Since the pollutant concentration is very significant parameter in water treatment process meanwhile, initial DNP concentration varied over a range from  $1.0 \times 10^{-3}$  mol dm<sup>-3</sup> to  $13.0 \times 10^{-3}$  mol dm<sup>-3</sup> (Fig. S2b). On increasing initial DNP concentration from  $1.0 \times 10^{-3}$  mol dm<sup>-3</sup> to  $7.0 \times 10^{-3}$  mol dm<sup>-3</sup>, rate constant increased from 0.022 to 0.087 min<sup>-1</sup> (Table S1). The scattering of light by excessive DNP present in water decreased rate constant above optimal value (Raizada et al., 2017a, 2017b). The rate constant was higher at initial reaction at pH 4.0 (Fig. S2c). The negative charge of Ag<sub>2</sub>CO<sub>3</sub>/PSGCN surface increased with increase in reaction pH while DNP had pK<sub>a</sub> respective value of 4.09. Above pK<sub>a</sub> value, DNP became negatively charged and released H<sup>+</sup> ions. It caused the poor adsorption of DNP onto Ag<sub>2</sub>CO<sub>3</sub>/PSGCN surface leading to reduction in photocatalytic activity. It was inferred that adsorption of DNP was maximal at lower pH.

### 3.2.4. Effect of H<sub>2</sub>O<sub>2</sub>, S<sub>2</sub>O<sub>8</sub><sup>2-</sup>, CO<sub>3</sub><sup>2-</sup>, Cl<sup>-</sup>, Fe<sup>3+</sup> and Cu<sup>2+</sup> ions on DNP degradation

The electron-hole pair recombination is one the foremost shortcoming sustained with photocatalyst. In the present work, photodegradation of DNP was investigated under H<sub>2</sub>O<sub>2</sub> and S<sub>2</sub>O<sub>8</sub><sup>2-</sup> that were used as electron scavenger (Fig. S3a and b). The deceptive rate increased from 0.089 min<sup>-1</sup> to 0.12 min<sup>-1</sup> on adding H<sub>2</sub>O<sub>2</sub> from  $1.0 \times 10^{-5}$  mol dm<sup>-3</sup> to  $7.0 \times 10^{-5}$  mol dm<sup>-3</sup>. Afterward, reaction rate reduced with increase in H<sub>2</sub>O<sub>2</sub> concentration and similar drift was perceived during DNP photodegradation in the presence of S<sub>2</sub>O<sub>8</sub><sup>2-</sup> ions with optimal concentration of  $7.0 \times 10^{-5}$  mol dm<sup>-3</sup> (Table 2). H<sub>2</sub>O<sub>2</sub> reacted photocatalytically in aqueous solution to produce hydroxyl radicals and improved reaction rate as shown by equations and also behaved as electron scavenger for photogenerated electron (Raizada et al., 2014a, 2014b).

S<sub>2</sub>O<sub>8</sub><sup>2-</sup> generated sulphate radical anion (SO<sub>4</sub><sup>·-</sup>) in water that eventually formed hydroxyl radicals (Table 2). The decrease in reaction rate above optimal concentration was because of scavenging of hydroxyl radical by H<sub>2</sub>O<sub>2</sub> whereas excessive adsorption of S<sub>2</sub>O<sub>8</sub><sup>2-</sup> ion condensed the photoactive volume. Fig. S3c and d showed the effect of CO<sub>3</sub><sup>2-</sup> and Cl<sup>-</sup> ions of DNP degradation and rate constant decreased from 0.084 min<sup>-1</sup> to 0.059 min<sup>-1</sup> with addition of different CO<sub>3</sub><sup>2-</sup> ion concentration ( $1.0 \times 10^{-3}$  mol dm<sup>-3</sup> to  $7.0 \times 10^{-3}$  mol dm<sup>-3</sup>) (Table 2). The addition of Cl<sup>-</sup> ions had destructive effect in photodegradation process. Scavenging of hydroxyl radicals by CO<sub>3</sub><sup>2-</sup> and Cl<sup>-</sup> ions lead to decrease in reaction rate (Raizada et al., 2017a, 2017b). On increasing Fe<sup>2+</sup> ion concentration from  $1.0 \times 10^{-3}$  mol dm<sup>-3</sup> to  $7.0 \times 10^{-3}$  mol dm<sup>-3</sup>, rate constant initially increased from 0.090 to 0.14 min<sup>-1</sup> (Fig. S3 e and f) and further increase in Fe<sup>2+</sup> ions concentration decreased rate constant. Cu<sup>2+</sup> ions also displayed similar trend like Fe<sup>2+</sup> ions. Both added Fe<sup>2+</sup>/Cu<sup>2+</sup> ions behaved as photogenerated electrons acceptor and reduced photogenerated electron-hole pair recombination (Mehdinia et al., 2012). The decrease in rate constant above optimal concentration was due to excessive adsorption of metal ion on photocatalyst surface that eventually minimized photoactive volume during photocatalytic process.

**Table 2** Effect of various ions of photodegradation of phenol degradation.

H <sub>2</sub> O <sub>2</sub>	Conc. (10 <sup>-5</sup> mol dm <sup>-3</sup> )	1.0	3.0	5.0	7.0	9.0	11.0	13.0
	k <sub>1</sub> (min <sup>-1</sup> )	0.087	0.092	0.096	0.11	0.093	0.089	0.083
S <sub>2</sub> O <sub>8</sub> <sup>2-</sup>	Conc. (10 <sup>-5</sup> mol dm <sup>-3</sup> )	1.0	3.0	5.0	7.0	9.0	11.0	13.0
	k <sub>1</sub> (min <sup>-1</sup> )	0.088	0.092	0.094	0.12	0.091	0.086	0.083
CO <sub>3</sub> <sup>2-</sup>	Conc. (10 <sup>-3</sup> mol dm <sup>-3</sup> )	1.0	3.0	5.0	7.0	9.0	11.0	13.0
	k <sub>1</sub> (min <sup>-1</sup> )	0.083	0.080	0.077	0.073	0.069	0.062	0.054
Cl <sup>-</sup>	Conc. (10 <sup>-3</sup> mol dm <sup>-3</sup> )	1.0	3.0	5.0	7.0	9.0	11.0	13.0
	k <sub>1</sub> (min <sup>-1</sup> )	0.081	0.078	0.076	0.072	0.071	0.065	0.062
Fe <sup>3+</sup>	Conc. (10 <sup>-4</sup> mol dm <sup>-3</sup> )	1.0	3.0	5.0	7.0	9.0	11.0	13.0
	k <sub>1</sub> (min <sup>-1</sup> )	0.091	0.090	0.095	0.16	0.092	0.089	0.083
Cu <sup>2+</sup>	Conc. (10 <sup>-4</sup> mol dm <sup>-3</sup> )	1.0	3.0	5.0	7.0	9.0	11.0	13.0
	k <sub>1</sub> (min <sup>-1</sup> )	0.090	0.093	0.097	0.14	0.090	0.087	0.082

Reaction parameters: [DNP] = 1 × 10<sup>-3</sup> mol dm<sup>-3</sup>; [DNP] = 1 × 10<sup>-4</sup> mol dm<sup>-3</sup>; [catalyst] = 50 mg/100 mL; initial reaction pH = 4.0; Time = 120 min. and Solar light intensity = 750 lx.

### 3.2.5. Mineralization ability and recyclability

The mineralization ability and recyclability of photocatalyst are important parameters for real time application of photocatalyst. Ag<sub>2</sub>CO<sub>3</sub>/PSGCN photocatalyst removed 99% of COD during mineralization of DNP in 6 h (Fig. 10a). Whereas PSGCN and Ag<sub>2</sub>CO<sub>3</sub> had 56 and 54% of COD reduction. These results indicated higher mineralization ability of Ag<sub>2</sub>CO<sub>3</sub>/PSGCN nanocomposite than PSGCN and Ag<sub>2</sub>CO<sub>3</sub>. CO<sub>2</sub> evolution throughout photodegradation process was due to mineralization of DNP into CO<sub>2</sub> and H<sub>2</sub>O (Fig. 10b). The time profile for HPLC analysis of degraded DNP is given

in Fig. 10c. The decrease in peak intensity at retention time (5 min) was noted for DNP (Fig. 10c) (Andrade et al., 2006). A group of fresh peaks was observed between retention time 2–4 min and disappeared after 8 h of reaction time. The presence of these peaks was assigned to degradation of DNP into simpler low molecular weight compounds. Additionally, liquid chromatography-mass spectrometry (LC-MS) was used to identify intermediate formation (Fig. 10d). The peaks for DNP were recorded at *m/z* ratio 110 (hydroquinone/resorcinol/catechol), 108 (benzoquinone), 118 (succinic acid), 116 (maleic acid), 90 (oxalic acid), and 46 (formic acid) and these

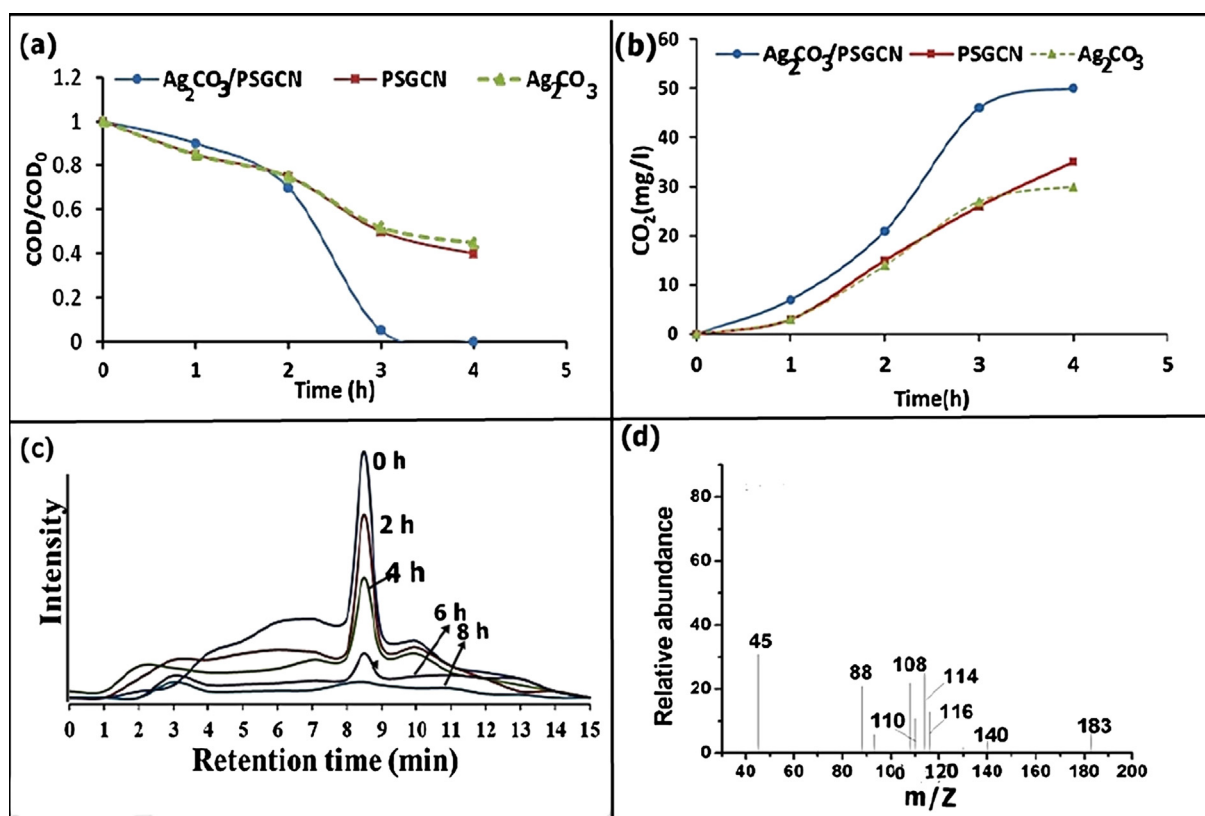


**Fig. 10** (a) COD and (b) CO<sub>2</sub> estimation during mineralization process. (c) HPLC and (d) LCMS analysis during degradation of DNP. [DNP] = 1.0 × 10<sup>-3</sup> mol dm<sup>-3</sup>; [photocatalyst] = 50 mg/100 mL; initial reaction pH = 4.0 and Light intensity = 750 lx.

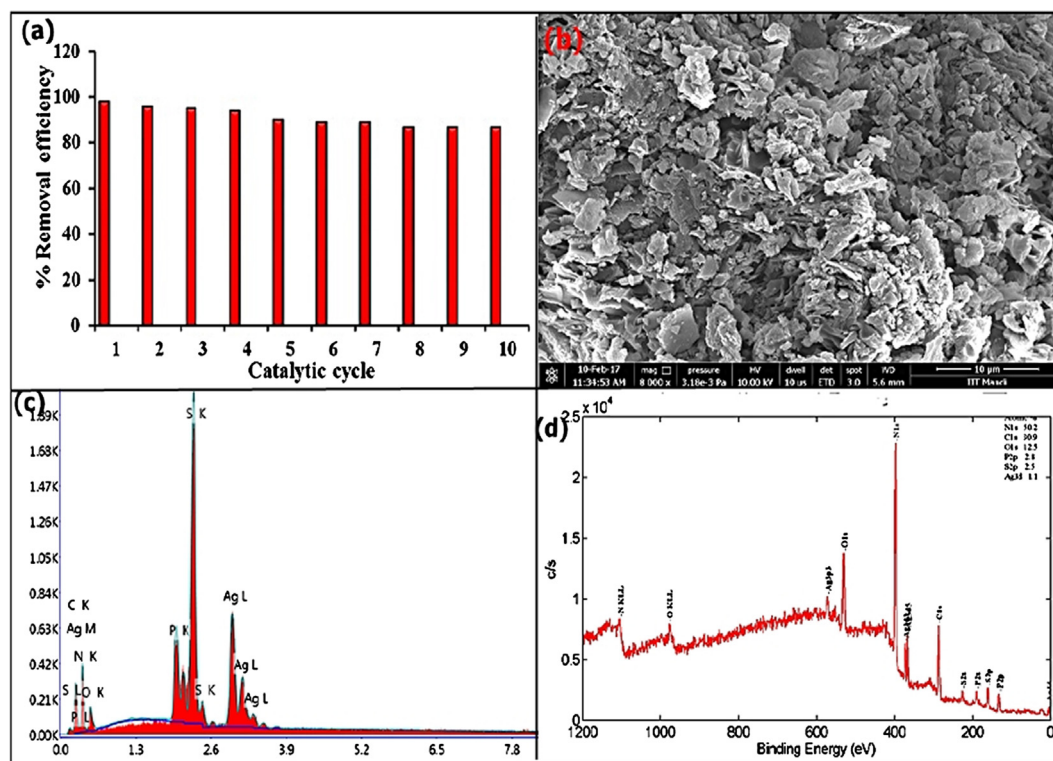


**Fig. 11** (a) Recycle efficiency of Ag<sub>2</sub>CO<sub>3</sub>/PSGCN photocatalyst, (b–d) SEM, EDX and XPS image after ten catalytic cycles. DNP] =  $1.0 \times 10^{-3}$  mol dm<sup>-3</sup>; [photocatalyst] = 50 mg/100 mL; initial reaction pH = 4.0 and Light intensity = 750 lx; reaction time = 120 min.

intermediates confirmed complete degradation of DNP (Shandilya et al., 2018a, 2018b, 2018c; Ahmed et al., 2010). Recyclability of photocatalyst is very crucial for real time applicability of photocatalyst. (Fig. 11a–d). After ten cycles, Ag<sub>2</sub>CO<sub>3</sub>/PSGCN nanocomposite had efficiency 87%. While no significant changes SEM, EDX and XPS spectra of Ag<sub>2</sub>CO<sub>3</sub>/PSGCN were noticed. This confirmed the stability of Ag<sub>2</sub>CO<sub>3</sub>/PSGCN as photocatalyst for DNP degradation.

#### 4. Conclusion

Ag<sub>2</sub>CO<sub>3</sub>/PSGCN photocatalyst with improved photocatalytic activity was successfully synthesized and applied for wastewater remediation. The P and S co-doping of g-C<sub>3</sub>N<sub>4</sub> lowered band gap of photocatalyst leading higher visible light activity. FESEM and TEM images showed deposition of Ag<sub>2</sub>CO<sub>3</sub> on PSGCN surface. XRD, XPS and FTIR analysis further validated the formation of heterojunction between Ag<sub>2</sub>CO<sub>3</sub> and PSGCN. AFM analysis verified successful formation sheet like structure of Ag<sub>2</sub>CO<sub>3</sub>/PSGCN nanocomposite to form stable suspension in water. Ag<sub>2</sub>CO<sub>3</sub>/PSGCN nanocomposite efficiently degraded DNP in 2 h involving pseudo first order kinetics and rate constants values of Ag<sub>2</sub>CO<sub>3</sub>/PSGCN were two times higher than bare PSGCN and Ag<sub>2</sub>CO<sub>3</sub>·H<sub>2</sub>O<sub>2</sub> and S<sub>2</sub>O<sub>8</sub><sup>2-</sup>, both had synergistic effect on DNP degradation while addition of CO<sub>3</sub><sup>2-</sup> and Cl<sup>-</sup> ions minimized rate constants for DNP degradation. Nearly, 99% of COD was removed in 6 h under visible light. Hydroxyl radicals (OH<sup>•</sup>) and holes (h<sub>vB</sub><sup>+</sup>) were main reactive species accountable for DNP degradation. No significant decrease in catalytic activity of Ag<sub>2</sub>CO<sub>3</sub>/

PSGCN nanocomposite was recorded for consecutive 10 cycles.

#### Appendix A. Supplementary material

Supplementary data to this article can be found online at <https://doi.org/10.1016/j.arabj.2018.10.004>.

#### References

- Adams, R.J., Blaedel, W.J., 1959. Electrodeposition of silver and copper without the use of cyanide. *J. Chem. Educ.* 36 (6), 286.
- Ahmed, S., Rasul, M.G., Martens, W.N., Brown, R., Hashib, M.A., 2010. Heterogeneous photocatalytic degradation of phenols in wastewater: a review on current status and developments. *Desalination* 261 (1–2), 3–18.
- Andrade, L.S., Laurindo, E.A., Oliveira, R.V.D., Rocha-Filho, R.C., Cass, Q.B., 2006. Development of a HPLC method to follow the degradation of phenol by electrochemical or photo-electrochemical treatment. *J. Braz. Chem. Soc.* 17 (2), 369–373.
- APHA, 1985. *Standard Methods for Examination of Water and Wastewater*. American Public Health Association, American Water Works Association, Water Environment Federation New York, p. 535.
- Bigelow, R.W., 1988. An XPS study of air corona discharge-induced corrosion products at Cu, Ag and Au ground planes. *Appl. Surf. Sci.* 32, 122–140.
- Bu, Y., Ren, J., Zhang, H., Yang, D., Chen, Z., Ao, J.P., 2018. Photogenerated-carrier separation along edge dislocation of WO<sub>3</sub> single-crystal nanoflower photoanode. *J. Mater. Chem. A* 6, 8604–8611.

- Cao, S., Huang, Q., Zhu, B., Yu, J., 2017. Trace-level phosphorus and sodium co-doping of g-C<sub>3</sub>N<sub>4</sub> for enhanced photocatalytic H<sub>2</sub> production. *J. Power Sources* 351, 151–159.
- Chen, J., Zhong, J., Li, J., Huang, S., Hu, W., Li, M., Du, Q., 2017. Synthesis and characterization of novel Ag<sub>2</sub>CO<sub>3</sub>/g-C<sub>3</sub>N<sub>4</sub> composite photocatalysts with excellent solar photocatalytic activity and mechanism insight. *Mol. Catal.* 435, 91–98.
- Dai, G., Yu, J., Liu, G., 2012. A new approach for photocorrosion inhibition of Ag<sub>2</sub>CO<sub>3</sub> photocatalyst with highly visible-light-responsive reactivity. *J. Phys. Chem. C* 116 (29), 15519–15524.
- Dong, C., Jiang, B.B., Wu, K.L., Hu, Y., Xia, S.H., Wei, X.W., 2015. Synthesis of nitrogen-doped graphene–Ag<sub>2</sub>CO<sub>3</sub> composites with enhanced photocatalytic efficiency. *Mater. Lett.* 146, 37–39.
- Dong, C., Wu, K.L., Wei, X.W., Li, X.Z., Liu, L., Ding, T.H., Wang, J., Ye, Y., 2014. Synthesis of graphene oxide–Ag<sub>2</sub>CO<sub>3</sub> composites with improved photoactivity and anti-photocorrosion. *Cryst. Eng. Comm.* 16, 730–736.
- Ge, L., Han, C., 2012. Synthesis of MWNTs/g-C<sub>3</sub>N<sub>4</sub> composite photocatalysts with efficient visible light photocatalytic hydrogen evolution activity. *Appl. Catal. B Environ.* 117–118, 268.
- Guo, S., Deng, Z., Li, M., Jiang, B., Tian, C., Pan, Q., Fu, H., 2016. Phosphorus-doped carbon nitride tubes with a layered micro-nanostructure for enhanced visible-light photocatalytic hydrogen evolution. *Angew. Chem. Int. Ed.* 128 (5), 1862–1866.
- He, H., Xue, S., Wu, Z., Yu, C., Yang, K., Peng, G., Zhou, W., Li, D., 2016. Sonochemical fabrication, characterization and enhanced photocatalytic performance of Ag<sub>2</sub>S/Ag<sub>2</sub>WO<sub>4</sub> composite micro-rods. *Chin. J. Catal.* 37 (11), 1841–1850.
- Hong, J., Xia, X., Wang, Y., Xu, R., 2012. Mesoporous carbon nitride with in situ sulfur doping for enhanced photocatalytic hydrogen evolution from water under visible light. *J. Mater. Chem.* 22 (30), 15006–15012.
- Hu, C., Hung, W.Z., Wang, M.S., Lu, P.J., 2018. Phosphorus and sulfur co-doped g-C<sub>3</sub>N<sub>4</sub> as an efficient metal-free photocatalyst. *Carbon* 127, 374–383.
- Hu, S.Z., Ma, L., You, J.G., Li, F.Y., Fan, Z.P., Wang, F., Liu, D., Gui, J.Z., 2014. A simple and efficient method to prepare phosphorus modified g-C<sub>3</sub>N<sub>4</sub> visible light photocatalyst. *RSC Adv.* 4 (41), 21657–21663.
- Hu, S., Ma, L., Xie, Y., Li, F., Fan, Z., Wang, F., Wang, Q., Wang, Y., Kang, X., Wu, G., 2015. Hydrothermal synthesis of oxygen functionalized S-P co-doped g-C<sub>3</sub>N<sub>4</sub> nanorods with outstanding visible light activity under anoxic conditions. *Dalton Tran.* 44 (48), 20889–20897.
- Jiang, J., Cao, S., Hu, C., Chen, C., 2017a. A comparison study of alkali metal-doped g-C<sub>3</sub>N<sub>4</sub> for visible-light photocatalytic hydrogen evolution. *Chin. J. Catal.* 38 (12), 1981–1989.
- Jiang, J., Li, H., Zhang, L., 2012. New insight into daylight photocatalysis of AgBr@ Ag: synergistic effect between semiconductor photocatalysis and plasmonic photocatalysis. *Chem. A Eur. J.* 18 (20), 6360–6369.
- Jiang, L., Yuan, X., Zeng, G., Chen, X., Wu, Z., Liang, J., Wang, H., Wang, H., 2017b. Phosphorus and sulfur co-doped g-C<sub>3</sub>N<sub>4</sub>: facile preparation, mechanism insight, and application as efficient photocatalyst for tetracycline and methyl orange degradation under visible light irradiation. *ACS Sustain. Chem. Eng.* 5 (7), 5831–5841.
- Jing, L., Xu, Y., Qin, C., Liu, J., Huang, S., He, M., Xu, H., Li, H., 2017. Visible-light-driven ZnFe<sub>2</sub>O<sub>4</sub>/Ag/Ag<sub>3</sub>VO<sub>4</sub> photocatalysts with enhanced photocatalytic activity under visible light irradiation. *Mater. Res. Bull.* 95, 607–615.
- Kim, J., Lee, C.W., Choi, W., 2010. Platinized WO<sub>3</sub> as an environmental photocatalyst that generates OH radicals under visible light. *Environ. Sci. Technol.* 44 (17), 6849–6854.
- Lakhi, K.S., Park, D.H., Al-Bahily, K., Cha, W., Viswanathan, B., Choy, J.H., Vinu, A., 2017. Mesoporous carbon nitrides: synthesis, functionalization, and applications. *Chem. Soc. Rev.* 46 (1), 72–101.
- Li, B., Hao, Y., Zhang, B., Shao, X., Hu, L., 2017. A multifunctional noble-metal-free catalyst of CuO/TiO<sub>2</sub> hybrid nanofibers. *Appl. Catal. A: Gen.* 531, 1–12.
- Li, B., Shao, X., Liu, T., Shao, L., Zhang, B., 2016. Construction of metal/WO<sub>2-72</sub>/rGO ternary nanocomposites with optimized adsorption, photocatalytic and photoelectrochemical properties. *Appl. Catal. B: Environ.* 198, 325–333.
- Li, J., Fang, W., Yu, C., Zhou, W., Xie, Y., 2015a. Ag-based semiconductor photocatalysts in environmental purification. *Appl. Surf. Sci.* 358, 46–56.
- Li, J., Wei, L., Yu, C., Fang, W., Xie, Y., Zhou, W., Zhu, L., 2015b. Preparation and characterization of graphene oxide/Ag<sub>2</sub>CO<sub>3</sub> photocatalyst and its visible light photocatalytic activity. *Appl. Surf. Sci.* 358, 168–174.
- Li, Y., Fang, L., Jin, R., Yang, Y., Fang, X., Xing, Y., Song, S., 2015c. Preparation and enhanced visible light photocatalytic activity of novel g-C<sub>3</sub>N<sub>4</sub> nanosheets loaded with Ag<sub>2</sub>CO<sub>3</sub> nanoparticles. *Nanoscale* 7 (2), 758–764.
- Liu, G., Niu, P., Sun, C., Smith, S.C., Chen, Z., Lu, G.Q., Cheng, H. M., 2010. Unique electronic structure induced high photoreactivity of sulfur-doped graphitic C<sub>3</sub>N<sub>4</sub>. *J. Am. Chem. Soc.* 132, 11642–11648.
- Maeda, K., Wang, X., Nishihara, Y., Lu, D., Antonietti, M., Domen, K., 2009. Photocatalytic activities of graphitic carbon nitride powder for water reduction and oxidation under visible light. *J. Phys. Chem. C* 113 (12), 4940–4947.
- Malik, R., Tomer, V.K., Chaudhary, V., Dahiya, M.S., Sharma, A., Nehra, S.P., Duhan, S., Kailasam, K., 2017. An excellent humidity sensor based on In–SnO<sub>2</sub> loaded mesoporous graphitic carbon nitride. *J. Mater. Chem. A* 5 (27), 14134–14143.
- Malik, R., Tomer, V.K., Dankwort, T., Mishra, Y.K., Kienle, L., 2018. Cubic mesoporous Pd–WO<sub>3</sub> loaded graphitic carbon nitride (g-CN) nanohybrids: highly sensitive and temperature dependent VOC sensors. *J. Mater. Chem. A* 2018 (6), 10718–10730.
- Mehdinia, A., Ahmadifar, M., Aziz-Zanjani, M.O., Jabbari, A., Hashtroudi, M.S., 2012. Selective adsorption of 2, 4-dinitrophenol on molecularly imprinted nanocomposites of mesoporous silica SBA-15/polyaniline. *Analyst* 137 (18), 4368–4374.
- Mousavi, M., Habibi-Yangjeh, A., Pouran, S.R., 2018. Review on magnetically separable graphitic carbon nitride-based nanocomposites as promising visible-light-driven photocatalysts. *J. Mater. Sci: Mater. Electron* 29, 1719–1747.
- Pare, B., Singh, P., Jonnalagadda, S.B., 2008. Visible light induced heterogeneous advanced oxidation process to degrade pararosanilin dye in aqueous suspension of ZnO. *Ind. J. Chem. Sect. A* 47 (6), 830–835.
- Pare, B., Singh, P., Jonnalagadda, S.B., 2009. Degradation and mineralization of victoria blue B dye in a slurry photoreactor using advanced oxidation process. *J. Sci. Ind. Res.* 68 (8), 724–729.
- Priya, B., Raizada, P., Singh, N., Thakur, P., Singh, P., 2016. Adsorptional photocatalytic mineralization of oxytetracycline and ampicillin antibiotics using Bi<sub>2</sub>O<sub>3</sub>/BiOCl supported on graphene sand composite and chitosan. *Colloid Interface Sci.* 479, 271–283.
- Raizada, P., Kumari, J., Shandilya, P., Dhiman, R., Singh, V.P., Singh, P., 2017a. Magnetically retrievable Bi<sub>2</sub>WO<sub>6</sub>/Fe<sub>3</sub>O<sub>4</sub> immobilized on graphene sand composite for investigation of photocatalytic mineralization of oxytetracycline and ampicillin. *Proc. Saf. Environ. Prot.* 106, 104–116.
- Raizada, P., Kumari, J., Shandilya, P., Singh, P., 2017b. Kinetics of photocatalytic mineralization of oxytetracycline and ampicillin using activated carbon supported ZnO/ZnWO. *Desalination* 79, 204–213.
- Raizada, P., Priya, B., Thakur, P., Singh, P., 2016. Solar light induced photodegradation of oxytetracycline using Zr doped TiO<sub>2</sub>/CaO based nanocomposite. *Ind. J. Chem. Sec. A* 55 (7), 803–809.
- Raizada, P., Singh, P., Kumar, A., Pare, B., Jonnalagadda, S.B., 2014a. Zero valent iron-brick grain nanocomposite for enhanced

- solar-Fenton removal of malachite green. *Sep. Purif. Technol.* 133, 429–437.
- Raizada, P., Singh, P., Kumar, A., Sharma, G., Pare, B., Jonnalagadda, S.B., Thakur, P., 2014b. Solar photocatalytic activity of nano-ZnO supported on activated carbon or brick grain particles: role of adsorption in dye degradation. *Appl. Catal. A* 486, 159–169.
- Ren, H.T., Jia, S.Y., Wu, S.H., Zhang, T.H., Han, X., 2015. Phase transformation synthesis of novel Ag<sub>2</sub>O/Ag<sub>2</sub>CO<sub>3</sub>/g-C<sub>3</sub>N<sub>4</sub> composite with enhanced photocatalytic activity. *Mater. Lett.* 142, 15–18.
- Rosman, N., Salleh, W.N.W., Ismail, A.F., Jaafar, J., Harun, Z., Aziz, F., Mohamed, M.A., Ohtani, B., Takashima, M., 2018. Photocatalytic degradation of phenol over visible light active ZnO/Ag<sub>2</sub>CO<sub>3</sub>/Ag<sub>2</sub>O nanocomposites heterojunction. *J. Photochem. Photobio. A: Chem.* 364, 602–612.
- Shandilya, P., Mittal, D., Kumar, M., Raizada, P., Hosseini-Bandegharaee, A., Saini, A.K., Singh, P., 2018a. Fabrication of fluorine doped graphene and SmVO<sub>4</sub> based dispersed and adsorptive photocatalyst for abatement of phenolic compounds from water and bacterial disinfection. *J. Cleaner Prod.* 203, 386–389.
- Shandilya, P., Mittal, D., Soni, M., Raizada, P., Lim, J.H., Jeong, D. Y., Dewedi, R.P., Saini, A.K., Singh, P., 2018b. Islanding of EuVO<sub>4</sub> on high-dispersed fluorine doped few layered graphene sheets for efficient photocatalytic mineralization of phenolic compounds and bacterial disinfection. *J. Taiwan Inst. Chem. Eng.*
- Shandilya, P., Mittal, D., Sudhaik, A., Soni, M., Raizada, P., Saini, A. K., Singh, P., 2018c. GdVO<sub>4</sub> modified fluorine doped graphene nanosheets as dispersed photocatalyst for mitigation of phenolic compounds in aqueous environment and bacterial disinfection. *Sep. Purif. Technol.* 2019, 804–816.
- Singh, P., Raizada, P., Kumari, S., Kumar, A., Pathania, D., Thakur, P., 2014. Solar-Fenton removal of malachite green with novel FeO-activated carbon nanocomposite. *Appl. Catal. A: General* 476, 9–18.
- Song, Y., Zhu, J., Xu, H., Wang, C., Xu, Y., Ji, H., Wang, K., Zhang, Q., Li, H., 2014. Synthesis, characterization and visible-light photocatalytic performance of Ag<sub>2</sub>CO<sub>3</sub> modified by graphene-oxide. *J. Alloy. Compd.* 592, 258–265.
- Sudhaik, A., Raizada, P., Shandilya, P., Jeong, D.Y., Lim, J.H., Singh, P., 2018a. Review on fabrication of graphitic carbon nitride based efficient nanocomposites for photodegradation of aqueous phase organic pollutants. *J. Ind. Eng. Chem.* 67 (25), 28–51.
- Sudhaik, A., Raizada, P., Shandilya, P., Singh, P., 2018b. Magnetically recoverable graphitic carbon nitride and NiFe<sub>2</sub>O<sub>4</sub> based magnetic photocatalyst for degradation of oxytetracycline antibiotic in simulated wastewater under solar light. *J. Environ. Chem. Eng.* 6 (4), 3874–3883.
- Sun, C., Zhang, H., Liu, H., Zheng, X., Zou, W., Dong, L., Qi, L., 2018. Enhanced activity of visible-light photocatalytic H<sub>2</sub> evolution of sulfur-doped g-C<sub>3</sub>N<sub>4</sub> photocatalyst via nanoparticle metal Ni as cocatalysts. *Appl. Catal. B Environ.* 235, 66–74.
- Tian, H., Zhang, X., Bu, Y., 2018. Sulfur-and carbon-codoped carbon nitride for photocatalytic hydrogen evolution performance improvement. *ACS Sustain. Chem. Eng.* 6 (6), 7346–7354.
- Tian, J., Liu, R., Liu, Z., Yu, C., Liu, M., 2017a. Boosting the photocatalytic performance of Ag<sub>2</sub>CO<sub>3</sub> crystals in phenol degradation via coupling with trace N-CQDs. *Chin. J. Catal.* 38, 1999–2008.
- Tian, J., Wu, Z., Liu, Z., Yu, C., Yang, K., Zhu, L., Huang, W., Zhou, Y., 2017b. Low-cost and efficient visible-light-driven CaMg (CO<sub>3</sub>)<sub>2</sub>@Ag<sub>2</sub>CO<sub>3</sub> microspheres fabricated via an ion exchange route. *Chin. J. Catal.* 38, 1899–1908.
- Tian, N., Huang, H., He, Y., Guo, Y., Zhang, Y., 2015. Organic-inorganic hybrid photocatalyst g-C<sub>3</sub>N<sub>4</sub>/Ag<sub>2</sub>CO<sub>3</sub> with highly efficient visible-light-active photocatalytic activity. *Colloids Surf. A: Physicochem. Eng. Aspects* 467, 188–194.
- Wang, S., Li, C., Wang, T., Zhang, P., Li, A., Gong, J., 2014a. Controllable synthesis of nanotube-type g-C<sub>3</sub>N<sub>4</sub> and their visible-light photocatalytic and fluorescent properties. *J. Mater. Chem. A* 2 (9), 2885–2890.
- Wang, S., Li, D., Sun, C., Yang, S., Guan, Y., He, H., 2014b. Synthesis and characterization of g-C<sub>3</sub>N<sub>4</sub>/Ag<sub>3</sub>VO<sub>4</sub> composites with significantly enhanced visible-light photocatalytic activity for triphenylmethane dye degradation. *Appl. Catal. B: Environ.* 144, 885–892.
- Wang, X., Li, S., Ma, Y., Yu, H., Yu, J., 2011. H<sub>2</sub>WO<sub>4</sub>·H<sub>2</sub>O/Ag/AgCl composite nanoplates: a plasmonic Z-scheme visible-light photocatalyst. *J. Phys. Chem. C* 115 (30), 14648–14655.
- Wang, X., Maeda, K., Thomas, A., Takanabe, K., Xin, G., Carlsson, J.M., Domen, K., Antonietti, M., 2009. A metal-free polymeric photocatalyst for hydrogen production from water under visible light. *Nat. Mater.* 8 (1), 76.
- Wu, X., Chen, F., Wang, X., Yu, H., 2018. In situ one-step hydrothermal synthesis of oxygen-containing groups-modified g-C<sub>3</sub>N<sub>4</sub> for the improved photocatalytic H<sub>2</sub>-evolution performance. *Appl. Surf. Sci.* 427, 645–653.
- Xu, C., Liu, Y., Huang, B., Li, H., Qin, X., Zhang, X., Dai, Y., 2011. Preparation, characterization, and photocatalytic properties of silver carbonate. *Appl. Surf. Sci.* 257 (20), 8732–8736.
- Xu, H., Song, Y., Song, Y., Zhu, J., Zhu, T., Liu, C., Zhao, D., Zhang, Q., Li, H., 2014. Synthesis and characterization of g-C<sub>3</sub>N<sub>4</sub>/Ag<sub>2</sub>CO<sub>3</sub> with enhanced visible-light photocatalytic activity for the degradation of organic pollutants. *RSC Adv.* 4 (65), 34539–34547.
- Yang, Y., Guo, W., Guo, Y., Zhao, Y., Yuan, X., Guo, Y., 2014. Fabrication of Z-scheme plasmonic photocatalyst Ag@AgBr/g-C<sub>3</sub>N<sub>4</sub> with enhanced visible-light photocatalytic activity. *J. Hazard. Mater.* 271, 150–159.
- Yi, Z.G., Ye, J.H., Kikugawa, N., Kako, T., Ouyang, S.X., Stuart-Williams, H., Yang, H., Cao, J.Y., Luo, W.J., Li, Z.S., Liu, Y., Yi, R.L., 2010. An orthophosphate semiconductor with photo-oxidation properties under visible-light irradiation. *Nat. Mater.* 9, 559–564.
- Yu, C., Li, G., Kumar, S., Yang, K., Jin, R., 2014. Phase transformation synthesis of novel Ag<sub>2</sub>O/Ag<sub>2</sub>CO<sub>3</sub> heterostructures with high visible light efficiency in photocatalytic degradation of pollutants. *Adv. Mater.* 26 (6), 892–898.
- Zeng, M., Zeng, X., Peng, X., Zhua, Z., Liao, J., Liu, K., Wang, G., Lin, S., 2015. Improving photoelectrochemical performance on quantum dots co-sensitized TiO<sub>2</sub> nanotube arrays using ZnO energy barrier by atomic layer deposition. *Appl. Surf. Sci.* 358, 385–392.
- Yu, N., Dong, R., Liu, J., Huang, K., Geng, B., 2016. Synthesis of Ag/Ag<sub>2</sub>CO<sub>3</sub> heterostructures with high length-diameter ratios for excellent photoactivity and anti-photocorrosion. *RSC Adv.* 6 (106), 103938–103943.
- Zhang, J., Sun, J., Maeda, K., Domen, K., Liu, P., Antonietti, M., Fu, X.Z., Wang, X., 2011. Sulfur-mediated synthesis of carbon nitride: band-gap engineering and improved functions for photocatalysis. *Energy Environ. Sci.* 4 (3), 675–678.
- Zhang, L., Chen, X., Guan, J., Jiang, Y., Hou, T., Mu, X., 2013. Facile synthesis of phosphorus doped graphitic carbon nitride polymers with enhanced visible-light photocatalytic activity. *Mater. Res. Bull.* 48 (9), 3485–3491.
- Zhang, M., Bai, X., Liu, D., Wang, J., Zhu, Y., 2015. Enhanced catalytic activity of potassium-doped graphitic carbon nitride induced by lower valence position. *Appl. Catal. B: Environ.* 164, 77–81.
- Zhang, Y., Mori, T., Ye, J., Antonietti, M., 2010. Phosphorus-doped carbon nitride solid: enhanced electrical conductivity and photocurrent generation. *J. Am. Chem. Soc.* 132 (18), 6294–6295.
- Zhu, J., Xiao, P., Li, H., Carabineiro, S.A., 2014. Graphitic carbon nitride: synthesis, properties, and applications in catalysis. *ACS Appl. Mater. Interfaces* 6 (19), 16449–16465.